The International Journal of Advanced Manufacturing Technology (2020) 107:1337–1344
https://doi.org/10.1007/s00170-019-04775-y

ORIGINAL ARTICLE

Prediction of subsurface damage depth in rotary ultrasonic machining of glass BK7 with probability statistics

Dongxi Lv[1] · Mingda Chen[1] · Youqiang Yao[1] · Yue Zhao[1] · Gang Chen[1] · Yunfeng Peng[2] · Yingdan Zhu[1,3]

Received: 26 July 2019 / Accepted: 29 November 2019 / Published online: 27 February 2020
© Springer-Verlag London Ltd., part of Springer Nature 2020

Abstract
Subsurface damage (SSD) generated in rotary ultrasonic machining (RUM) process significantly deteriorates the technological and structural performance of the optical components. However, the invisibility of subsurface cracks underneath the machined surface makes it difficult to accurately and online evaluate the SSD depth. In the present research, incorporated with the probability statistics of the abrasive heights and the indentation fracture mechanics of the brittle material, a theoretical prediction model was established by investigating the inherent correlation between the measured cutting force of the diamond tool and the maximum depth of the subsurface cracks. Utilizing this predictive method, the SSD depth could be rapidly and precisely calculated through the mechanical properties of the material, the cutting force of the diamond tool, and the geometrical characteristics of the abrasives. To validate the feasibility of prediction technique, the experimental measurements of the maximum SSD depths were compared with the predicted results, revealing the acceptable consistency in their values.

Keywords Rotary ultrasonic machining · Cutting force · Subsurface damage · Theoretical prediction model · Glass BK7

1 Introduction

Abrasive machining techniques for initial shaping and figuring of the optical elements generally introduce the subsurface damage (SSD) concentrated on the final surface which refers to the elastic/plastic deformation and the residual subsurface cracks [1]. The presentation of subsurface cracks significantly affects the technological applications of the optical components, such as secular stability, operational durability, and laser-induced damage threshold [2]. Therefore, these residual cracks should be gradually diminished or even eliminated in the subsequent machining processes by optimizing the processing parameters [3]. The necessary prerequisite for the parameter optimization is the precise detection or prediction of the SSD depth to improve the subsurface quality and the processing efficiency.

Up to the present, massive destructive and nondestructive techniques have been proposed to examine the SSD depth of the machined components, which considerably benefit the optical fabrication. Typical nondestructive techniques including ultrasonic scanning microscopy, total internal reflection microscopy, X-ray diffraction method, and the improved white light interferometer [4, 5] were developed to quantitatively measure the subsurface crack depths rapidly without destroying the machined surfaces. While, these evaluation methods could only provide the qualitative measurements rather than the quantitative results of the SSD depth [6]. In this context, the low detection accuracy of the nondestructive means made it time-consuming to sufficient removal of the subsurface cracks in the subsequent procedures, thus significantly reducing the processing efficiency. Conversely, the destructive techniques, such as magnetorheological finishing (MRF) wedge, taper polishing, and chemical etching method, could precisely provide the fundamental information of the SSD topography and distribution by exposing the subsurface crack structures below the machined surface [3]. While, these physical modifications of the optical components would inevitably influence the final application of the finished surfaces, which were obviously unacceptable for the expensive optical elements. Furthermore, the measurements of the subsurface

✉ Yingdan Zhu
y.zhu@nimte.ac.cn

[1] Institute of Advanced Manufacturing Technology, Ningbo Institute of Material Technology and Engineering, Chinese Academy of Sciences, Zhongguan West Road 1219#, Ningbo 315201, People's Republic of China

[2] Department of Mechanical and Electrical Engineering, Xiamen University, Xiamen 3610005, People's Republic of China

[3] Center of Materials Science and Optoelectronics Engineering, University of Chinese Academy of Sciences, Beijing 100049, People's Republic of China

crack depth at the selected machining conditions could not entirely characterize the SSD depths of all the optical components, hereby distinctly reducing the measuring efficiency of the destructive methods.

Due to the disadvantages of the nondestructive and destructive estimation techniques, various non-linear/linear relationships between the surface roughness (SR) and subsurface crack depth were also developed based on the sufficient comprehension of the formation mechanisms of the lateral/median cracks. Thus, the SSD depth could be rapidly and indirectly estimated by measuring the SR of the machined surface, which significantly facilitates the manufacture of the optical components [7]. However, these evaluation methods exhibited some localizations for the in situ monitoring of subsurface quality. Therefore, Wang et al. proposed a non-linear theoretical correlation between the cutting force of the diamond tool and the SSD depth of the machined surface, realizing the online prediction of the subsurface crack depth [8]. This mechanistic prediction technique was grounded on the hypothesis that the abrasives situated on the tool end-face were all involved in the actual machining process. However, Hou and Komanduri mentioned that only 3.8% of the abrasives participated into the actual material removal process rather than all the abrasives [9]. Moreover, the stochastic distribution characteristics of the abrasives brought about the evident differences in their extrusion loads [9], which served to significantly affect the propagation depths of the induced cracks, while the stochastic properties of the abrasive sizes were discounted in the prediction method of Wang et al. [8].

In the present research, considering the indentation fracture mechanics of the brittle material, a theoretical prediction method for the SSD depth produced in rotary ultrasonic machining (RUM) process was proposed based on the probability statistics of the active machining abrasives. The prediction method intrinsically correlated the measured cutting force of the diamond tool with the maximum subsurface crack depth of the machined surface. Utilizing the mechanistic prediction, the SSD depth of the RUM surface could be precisely predicted or even in situ monitored. The nondestructive evaluation technique would benefit the improvement of the processing efficiency and the reduction of the processing costs.

2 Formation mechanisms of subsurface damage and determination of abrasive number

2.1 Formation mechanisms of subsurface cracks

Schematic illustration of the RUM process is presented in Fig. 1. A rotary core tool impregnated with the metal-bonded diamond abrasives was ultrasonically vibrated in the axial direction, meanwhile fed along the specimen surface at a constant speed. The internal coolant jetted through the central hole of the diamond tool, washing away the machining debris and cooling the diamond tool simultaneously. For each individual abrasive located on the boundary of the tool end-face, its primary movements could be decomposed into high-speed rotation, feeding motion, and ultrasonic vibration. Thus, the theoretical trajectory of the abrasive at the end-face border could be expressed as:

$$\begin{cases} S_x = r_{\text{outer}}\cos(\omega t) + v_f t \\ S_y = r_{\text{outer}}\sin(\omega t) \\ S_z = A\cos(2\pi f t) \end{cases} \tag{1}$$

where $\omega = \pi n/30$ is the rotational velocity, n is the rotation speed, v_f is the feeding speed, r_{outer} is outer semidiameter of the diamond tool, t is the processing time, and f and A are the frequency and amplitude of the ultrasonic vibration, respectively. According to Eq. 1, the abrasive trajectory in the circumferential direction of the diamond tool is presented in Fig. 2. Evidently, the superimposition of an ultrasonic vibration fundamentally altered the processing kinematics, leading to the abrasive traveled along the sinusoidal trajectory. Obviously, the periodic fluctuations in the specific trajectory brought about the intermittent interaction between the abrasive and the material. The contact interruption significantly shrunk the effective cutting time Δt^x of the abrasive:

$$\Delta t^x = \frac{1}{\pi f}\left[\frac{\pi}{2} - \arcsin\left(1 - \frac{\delta^x_{\max}}{A}\right)\right] \tag{2}$$

where $\delta^x_{\max}$ is the maximum cutting depth of the abrasive at the bottom of the track.

In the abrasive machining process, the mutual interactions between the abrasives and the material were generally likened to the small-scale indentation events with the numerous sharp indenters [10]. Thus, the indentation fracture mechanics of the brittle material could be employed to explore the formation mechanisms of subsurface cracks in formal RUM process. In

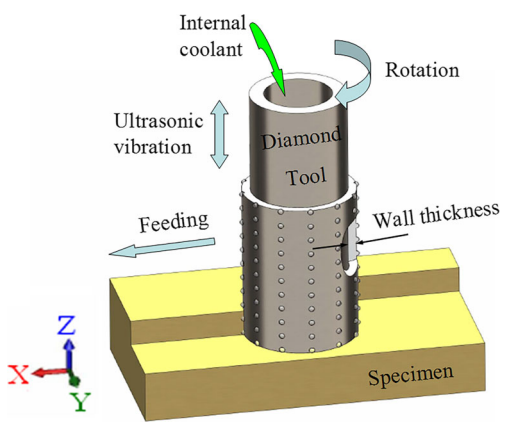

Fig. 1 Illustration of the rotary ultrasonic machining process

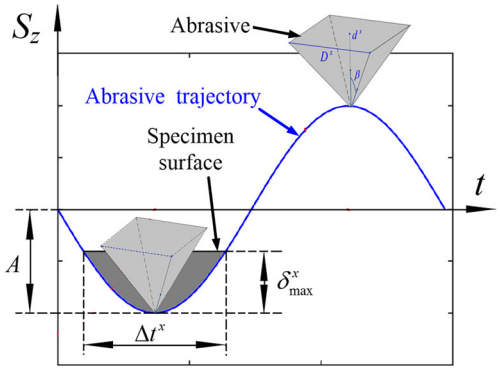

Fig. 2 Intermittence contact between the abrasive and the specimen surface

addition, numerous investigations on the morphological observations and dimension detections represented that the abrasives exhibited the irregular distribution features in the geometries and the grain sizes [11]. Hence, the present investigation simplified the abrasives on the tool end-face as the sharp pyramid indenters with the same geometry but different dimensions. For any abrasive, the length D^x of the pyramid edge was equivalent to its grain size, and the semi-angle between two opposite edges was $\beta = 45°$, as illustrated in Fig. 2. Thus, the abrasive height d^x could be deduced as:

$$d^x = \frac{\sqrt{2}D^x}{2\tan\beta}. \tag{3}$$

As depicted in Fig. 2, the periodic fluctuations in the sinusoidal trajectory of the abrasive caused its instantaneous cutting depth approached the maximum δ^x_{max} at the bottom of the trajectory. Presumably, the transient cutting force of the abrasive also reached the maximum F^x_{single} which could be calculated by the following equation [12]:

$$F^x_{single} = 2H_V \tan\beta \sqrt{\tan^2\beta + 2}\left(\delta^x_{max}\right)^2 \tag{4}$$

where H_V is the Vickers hardness of the material. Therefore, under the extrusion of F^x_{single}, the complex elastic/plastic deformations would emerge in the interior material underneath the contact site [13], as presented in Fig. 3. The median crack initially nucleated nearby the bottom of the plastic deformation boundary and propagated downwards in the form of full circle or truncated circular segment [14]. The final propagation length L^x_{median} of median crack could be considered as the subsurface damage (SSD) depth. Based on indentation fracture mechanics, Lambropoulos et al. developed the calculation formula of L^x_{median} [15]:

$$L^x_{median} = \alpha_k{}^{2/3}\left(\frac{E}{H_V}\right)^{(1-q)2/3}(\cot\beta)^{4/9}\left(\frac{F^x_{single}}{K_{IC}}\right)^{2/3} \tag{5}$$

where $q = 0.5$ is a dimensionless coefficient of correction, $\alpha_k = 0.027 + 0.090 \times (q - 1/3)$, E and K_{IC} are the elastic

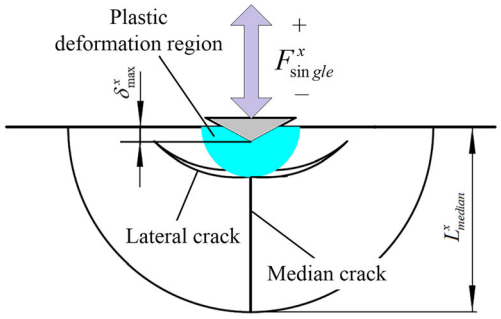

Fig. 3 Cracking systems evoked by the abrasive indentation

modulus and fracture toughness of the material, respectively. Considering Eqs. 4 and 5, it was obvious that L^x_{median} induced by a single abrasive was primarily determined by its δ^x_{max}.

In this research, the median crack depth/SSD depth L^x_{median} induced by the abrasive with δ^x_{max} was denoted as SSD^x (viz., $L^x_{median} = SSD^x$). Additionally, the visible differences in the abrasive heights served to distinctly affect their respective δ^x_{max} and F^x_{single} [16] and substantially influence the propagation depths of the median cracks. Consequently, under the combination effects of the abrasives with various heights, the subsurface cracks of the final surface exhibited the disorderly distribution characteristics, as detailed in Section 4.2.

2.2 Determination of abrasive number on end-face boundary

Extensive investigations on the modeling techniques of the SSD depth were grounded on the speculative hypothesis that the abrasives on the tool end-face all participated in the formations of the subsurface cracks [9]. However, the topographic observations of diamond tool after the formal RUM experiments indicated that only the abrasives at the end-face corner contributed to the actual material removal rather than all the abrasives on the end-face [17]. Moreover, Lv et al. demonstrated that the abrasive had the opportunity to make contribution to the material removal, only when its distance from the border was less than the average distance b between two neighboring abrasives [16], as presented in Fig. 4. Therefore, the total abrasives distributed at this specific region could be approximately regarded as the effective abrasive number N_{total} [16]:

$$N_{total} = \pi r_{outer}\left(\frac{0.88 \times 10^{-3} C_a}{100 \times \left(\sqrt{2}/(6\tan\beta)\right) \times \rho \times \overline{D}^3}\right)^{1/3} \tag{6}$$

where $C_a = 100$ is the abrasive concentration, $\rho = 3.52 \times 10^{-3} g/mm^3$ is the diamond density, $\overline{D} = (D_{max} + D_{min})/2$ is the average dimension of the abrasives, and D_{max} and D_{min} are the dimensions of the maximum and minimum abrasives which could be obtained by referring to the related manuals [18].

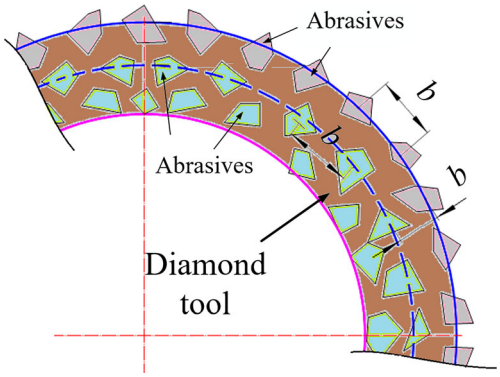

Fig. 4 Distribution characteristics of the abrasives situated on the tool end-face

3 Mechanistic prediction for subsurface damage depth

3.1 Intrinsic association between measured cutting force and maximum cutting depth of abrasives

The macroscopic cutting force of the diamond tool measured in formal RUM process could be generally considered as the aggregate effects of the extrusion loading induced by each active abrasive in microscopic perspective which essentially depended on the abrasive heights [9, 19]. Additionally, Hou and Komanduri mentioned that the abrasive heights d^x revealed the extremely irregular characteristics, and d^x followed the normal/Gaussian distribution [9]. Therefore, the probabilistic statistical methods could be adopted to calculate the total number of the abrasives at a specific height.

Probability distribution features of the abrasive heights are presented in Fig. 5. It was clearly seen that whether one abrasive could participate in the actual material removal depended not only on its height d^x ($d^x \in [d_{\min}, d_{\max}]$, and $d_{\min}/d_{\max}$ is the height of the minimum/maximum abrasive) but also on the equivalent indentation depth $d_{\text{ind}}^{\text{equ}}$ of the diamond tool. To facilitate differentiation, the height of the active machining abrasive was denoted as d_{mach}^x, and its maximum cutting depth was referred as $\delta_{\max}^x$. Apparently, the height of the minimum active abrasive $d_{\text{mach}}^{\min}$ could be given by:

$$d_{\text{mach}}^{\min} = d_{\max} - d_{\text{ind}}^{\text{equ}}. \tag{7}$$

Taking Eq. 7 and Fig. 5 into account, it could be deduced that the larger $d_{\text{ind}}^{\text{equ}}$ served to magnify the cutting depth of each active abrasive and also enlarge the relevant probability of the active abrasives (area of green region in Fig. 5). For any abrasive with the height d_{mach}^x, its $\delta_{\max}^x$ was ranged from 0 to $d_{\text{mach}}^{\min}$ (viz., $\delta_{\max}^x \in [0, d_{\text{mach}}^{\min}]$), and $\delta_{\max}^x$ could be expressed as:

$$\delta_{\max}^x = d_{\text{mach}}^x - d_{\text{mach}}^{\min}. \tag{8}$$

The statistical analysis on the abrasive dimensions conducted by Hou and Komanduri suggested that the abrasive heights followed the normal/Gaussian distribution [9], and distribution density could be calculated as:

$$y = \frac{1}{\sqrt{2\pi}} e^{-x^2/2} \tag{9}$$

where y is the variation of the frequency with respect to the independent variable x. When $x \in [p, +\infty]$ (see Fig. 5), the probability function $P(p)$ corresponding to the green region under the distribution curve could be achieved by integrating from p to $+\infty$:

$$P(p) = \frac{1}{\sqrt{2\pi}} \int_p^{+\infty} e^{-x^2/2} dx. \tag{10}$$

The probability distribution of the active abrasives with the height d_{mach}^x is depicted in Fig. 6. Evidently, the total number N_{mach}^x of these abrasives could be expressed as:

$$N_{\text{mach}}^x = N_{\text{total}} \times \frac{1}{\sqrt{2\pi}} e^{-x^2/2} dx. \tag{11}$$

In addition, for the active abrasive with the minimum height $d_{\text{mach}}^{\min}$, the corresponding value $x_{\text{mach}}^{\min}$ could be obtained as:

$$x_{\text{mach}}^{\min} = \frac{\Delta}{2} - d_{\text{ind}}^{\text{equ}} \tag{12}$$

where Δ is the difference between $d_{\max}$ and $d_{\min}$ (namely, $\Delta = d_{\max} - d_{\min}$).

As mentioned in Section 2.1, for one abrasive with d_{mach}^x, the periodic variation in its instantaneous cutting depth resulted in the abrasive-material extrusion load approached the maximum F_{single}^x at the bottom of the abrasive trajectory. Thus, the total loading F_{total}^x evoked by the extrusions of all these abrasives could be deduced as:

$$F_{\text{total}}^x = N_{\text{mach}}^x \times F_{\text{single}}^x. \tag{13}$$

Obviously, the summation of F_{total}^x for all the active abrasives with various heights was unequalized to the experimental measurement F which characterized the average cutting force of the diamond tool. Whereas, the impulse summation $\text{Impulse}_{\text{total}}$ of the total active abrasives was directly equivalent to that provoked by F during each ultrasonic cycle [20]. This conclusion provided a possibility to qualitatively associate F_{total}^x with F.

The total impulse $\text{Impulse}_{\text{total}}^x$ induced by all the abrasives with the height d_{mach}^x could be written as:

$$\text{Impulse}_{\text{total}}^x = F_{\text{total}}^x \Delta t^x. \tag{14}$$

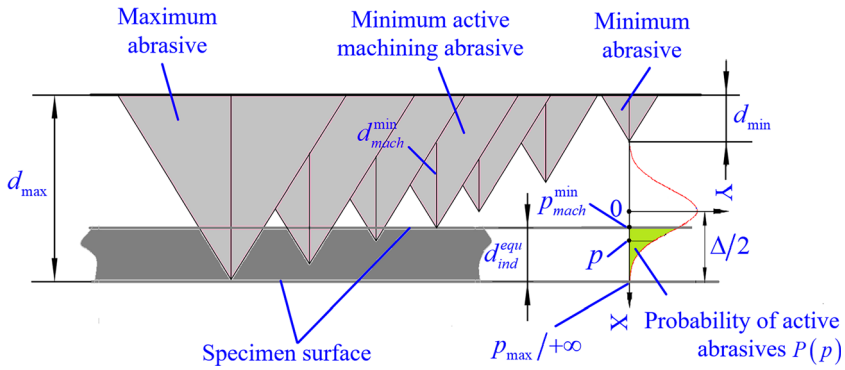

Fig. 5 Probability distribution of the abrasive heights and the active abrasives

Therefore, substituting of Eqs. 11 and 13 into Eq. 14, the impulse $\text{Impulse}_{\text{total}}$ of the diamond tool could be achieved by integrating Eq. 14 from $p_{\text{mach}}^{\min}$ to +∞, thus:

$$\text{Impulse}_{\text{total}} = \int_{p_{\text{mach}}^{\min}}^{+\infty} F_{\text{single}}^{x} \Delta t^{x} N_{\text{total}} \frac{1}{\sqrt{2\pi}} e^{-x^2/2} dx \tag{15}$$

where $p_{\text{mach}}^{\min}$ is the equivalent argument of $P(p)$ at $x_{\text{mach}}^{\min}$ which corresponded to the active abrasive with the minimum height $d_{\text{mach}}^{\min}$ [16]. Additionally, since $P(p)$ converged rapidly approaching zero when $x \geq 3$, a finite number 3 at point $p_{\max}$ (viz., $p_{\max} = 3$) could be considered as the upper limit +∞ of $P(p)$ for the minimal error (about 0.13%) [9]. In this context, $p_{\text{mach}}^{\min}$ could be expressed by the following equation (see Fig. 6):

$$p_{\text{mach}}^{\min} = \left(\frac{\Delta}{2} - d_{\text{ind}}^{\text{equ}}\right) \times \frac{3}{\Delta/2}. \tag{16}$$

In addition, $\text{Impulse}_{\text{total}}$ of the diamond tool could also be described in terms of F as:

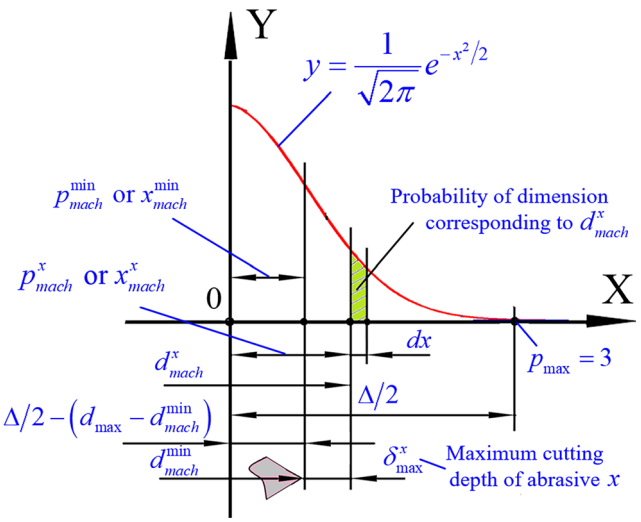

Fig. 6 Probability of abrasives corresponding to d_{mach}^{x} at $[d_{\text{mach}}^{\min}, d_{\max}]$ [16]

$$\text{Impulse}_{\text{total}} = \frac{1}{f} F \tag{17}$$

By equating Eqs. 15 and 17, the quantitative relation between F and F_{single}^{x} could be obtained as:

$$F = f \times N_{\text{total}} \times \int_{p_{\text{mach}}^{\min}}^{3} F_{\text{single}}^{x} \Delta t^{x} \frac{1}{\sqrt{2\pi}} e^{-x^2/2} dx \tag{18}$$

Evidently, the above intrinsic association incorporated the random distribution characteristics of the active abrasives on the end-face border of the diamond tool. To reduce the calculation complication of the intrinsic relationship, Eq. 2 could be simplified as [21]:

$$\Delta t^{x} \approx \frac{\delta_{\max}^{x}}{2Af} \tag{19}$$

Thus, substituting Eq. 19 into Eq. 18, the inherent correlation between F and $\delta_{\max}^{x}$ was developed as:

$$F = \frac{H_V \tan\beta N_{\text{total}} \sqrt{\tan^2\beta + 2}}{A\sqrt{2\pi}} \int_{p_{\text{mach}}^{\min}}^{3} \left(\delta_{\max}^{x}\right)^3 e^{-x^2/2} dx \tag{20}$$

Analogous to the achievement of $p_{\text{mach}}^{\min}$, substituting Eqs. 7, 8, and 12 into Eq. 16, the equivalent variable p_{mach}^{x} of $P(p)$ for the active abrasives with $\delta_{\max}^{x}$ (height d_{mach}^{x}) could be written as:

$$p_{\text{mach}}^{x} = \left[\delta_{\max}^{x} + \frac{\Delta}{2} - \left(d_{\max} - d_{\text{mach}}^{\min}\right)\right] \times \frac{3}{\Delta/2} \tag{21}$$

Substituting Eq. 21 into Eq. 20, F could be deduced as:

$$F = \frac{N_{\text{total}}}{A\sqrt{2\pi}} H_V \tan\beta \sqrt{\tan^2\beta + 2} \int_{p_{\text{mach}}^{\min}}^{3} \left(\frac{x\Delta}{6} - \frac{\Delta}{2} + \left(d_{\max} - d_{\text{mach}}^{\min}\right)\right)^3 e^{-x^2/2} dx \tag{22}$$

where $p_{\text{mach}}^{\min} = \left(\frac{\Delta}{2} - d_{\text{ind}}^{\text{equ}}\right) \times \frac{3}{\Delta/2}$. Obviously, Eq. 22 translated the measured cutting force F into a function of the equivalent indentation depth $d_{\text{ind}}^{\text{equ}}$ of the diamond tool.

Table 1 Specifications of the diamond tool [8]

Outer semidiameter r_{outer} (mm)	Wall thickness (mm)	Average grain size $\overline{D}$ (μm)	Diamond concentration C_a
5	1	91	100
Vibration amplitude A (μm)	Vibration frequency f (kHz)	Maximum grain size D_{max} (μm)	Minimum grain size D_{min} (μm)
15	17	106	75

3.2 Development of prediction model for SSD depth

As mentioned in Section 2.1, the active abrasives with their height d^x_{mach} penetrated the specimen surface with the maximum cutting depth δ^x_{max} which determined the propagation depth L^x_{median} of the median cracks [22]. Based on this intrinsic correlation, it could be speculated that the evident difference in the active abrasive heights would bring about the formations of the median cracks with various depths, which was responsible for the stochastic distribution attributes of the subsurface cracks, as detailed in Section 4.2. Furthermore, the inherent correspondence between d^x_{mach} and L^x_{median} also indicated that the subsurface crack with the maximum depth L^{max}_{median} was presumably provoked by the abrasive with the maximum height d_{max}. In this case, the maximum cutting depth δ^{max}_{max} of this specific abrasive was identical with the equivalent indentation depth d^{equ}_{ind} of the diamond tool at the selected machining parameters (viz., $\delta^{max}_{max} = d^{equ}_{ind}$).

Therefore, to establish the quantitative relationship between the measured cutting force F of the diamond tool and the theoretical maximum SSD depth SSD^{max}_{theo} of the machined surface, it was essential to firstly explore the intrinsic association between δ^{max}_{max} and L^{max}_{median}. Combining Eq. 4 and Eq. 5, $SSD^{max}_{theo}/L^{max}_{median}$ could be described by the following equation:

$$SSD^{max}_{theo} = {\alpha_k}^{2/3}\left(\frac{E}{H_V}\right)^{(1-q)2/3}(\cot\beta)^{4/9}\left(\frac{2H_V\tan\beta\sqrt{\tan^2\beta+2}}{K_{IC}}\right)^{2/3}\left(\delta^{max}_{max}\right)^{4/3} \quad (23)$$

where $\delta^{max}_{max} = d^{equ}_{ind}$. In addition, the present investigation presumed that the actual maximum SSD depth SSD^{max}_{actu} of the machined surface was proportional to its theoretical value SSD^{max}_{theo} with a proportionality parameter K and a constant l, namely $SSD^{max}_{actu} = K \times SSD^{max}_{theo} + l$. Noting that K and l considered the influence of the mutual overlapping of the abrasive tracks and the feeding motion of the diamond tool on d^{equ}_{ind}, which could be achieved by fitting a series of experimental data.

In conclusion, under the achievements of K and l values, d^{equ}_{ind} and SSD^{max}_{actu} were two unknown terms. Additionally, with the measurement F of the diamond tool, d^{equ}_{ind} could be achieved with Eq. 22. Since $SSD^{max}_{actu} = K \times SSD^{max}_{theo} + l$, SSD^{max}_{actu} could be predicted by solving Eqs. 22 and 23 simultaneously. Apparently, the established prediction method for the SSD depth characterized the maximum subsurface crack depth of the RUM surface.

4 Experimental verifications

4.1 Experimental apparatus and procedure

In this section, the experimental results from the literature [8] were considered to validate the developed predictive model for the SSD depth. The formal RUM experiments were performed on glass BK7 with a Sauer Ultrasonic 50 (DMG, Germany). The mechanical properties of glass BK7 at ambient temperature are the following: density $\rho = 2.52$ g/cm^3, Vickers hardness H_V = 7.2 GPa, Young's modulus E = 85.9 GPa, Poisson's ratio ν = 0.28, and fracture toughness K_{IC} = 0.8 MPa m$^{1/2}$ [8]. A core nickel-bonded tool with the diameter of 10 mm was selected for the verification experiments. The detailed specifications of the diamond tool and the processing parameters are tabulated in Tables 1 and 2, respectively.

4.2 Morphology observations of subsurface cracks

The typical SSD topographies produced in formal RUM process were arrayed with respect to the depth from the original machined surface, as illustrated in Fig. 7. It was evident that the crater-like defects and the subsurface cracks were both observed which were respectively induced by propagations of the lateral cracks and median cracks [7]. Crater-like topographies were just concentrated at the vicinity of the top surface (Fig. 7a), and their distribution density rapidly reduced with the depth increasing, leaving subsurface cracks dominated the

Table 2 Manufacturing parameters of the verification experiments [8]

Experiment	Rotation speed n (rpm)	Feed speed v_f (mm/min)	Cutting depth a_p (μm)
1st group	1000, 2000, 3000, 4000, 5000, 6000, 8000	6	60
2nd group	3000	2, 6, 8, 12, 16, 24	60

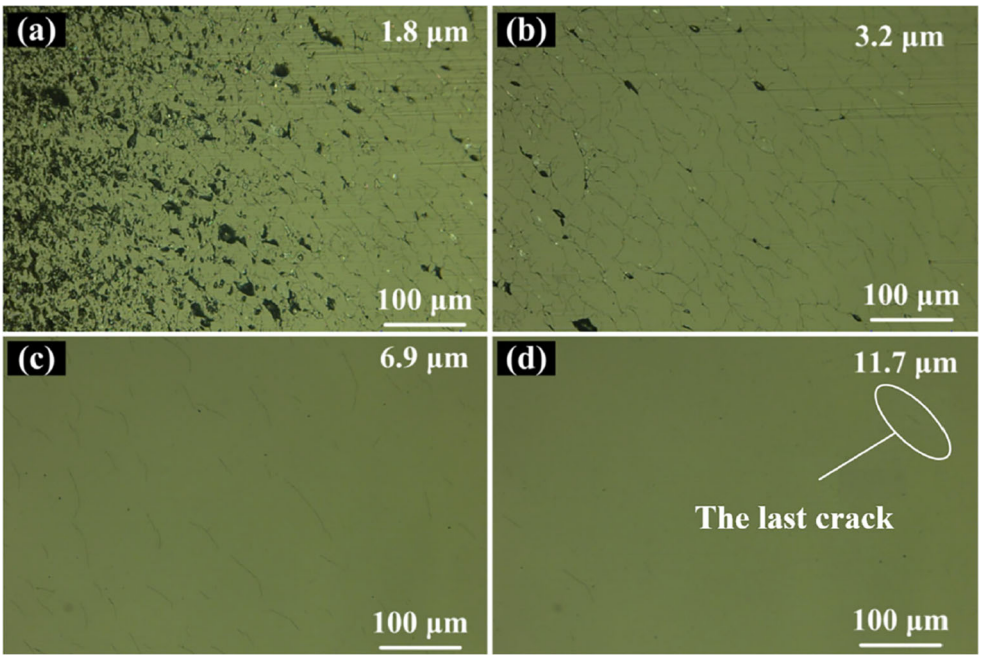

Fig. 7 Typical SSD micrographs of the machined surface at different depths [8]. **a** 1.8 μm. **b** 3.2 μm. **c** 6.9 μm. **d** 11.7 μm

SSD appearance. Furthermore, the disorderly subsurface cracks initially interconnected with each other and gradually became isolated with the increase of the depth (see Fig. 7b, c). This phenomenon might be interpreted in terms of the normal distribution characteristics of the active machining abrasives coupled with the inherent correspondence between the abrasive height d^x_{mach} and the median crack depth L^x_{median}. As described in Fig. 6 and Eq. 11, the total number N^x_{mach} of the active abrasives with any selected height d^x_{mach} presented a decreasing tendency with the abrasive height increasing. By this token, the active abrasives with the height about $d^{\min}_{\mathrm{mach}}$ had the largest number, thus leading to the formation of numerous median cracks with small depths. Therefore, the subsurface cracks adjacent to the top RUM surface exhibited the interconnected and disorder distribution characteristics (see Fig. 7a, b). With the increment of d^x_{mach}, N^x_{mach} was distinctly decreased. In this case, the propagation depths of the induced median cracks were visibly increased, while the crack density was correspondingly reduced, hereby causing the interconnected subsurface cracks generally isolated from each other, as exhibited in Fig. 7c. Finally, the isolated crack completely vanished after exceeding the depth of 11.7 μm which was regarded as the maximum SSD depth $\mathrm{SSD}^{\max}_{\mathrm{actu}}$ (Fig. 7d).

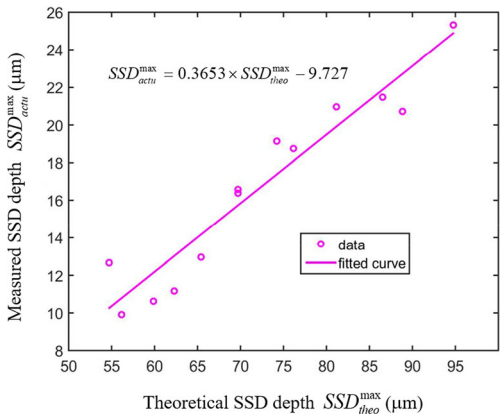

Fig. 8 Variation of the measured SSD depth $\mathrm{SSD}^{\max}_{\mathrm{actu}}$ with the corresponding theoretical value $\mathrm{SSD}^{\max}_{\mathrm{theo}}$

4.3 Verification of predictive SSD model

The theoretical prediction model of the SSD depth developed in Section 3 presupposed the parameters K and l independent of the processing parameters. To verify this hypothesis, with the tool specifications listed in Table 1 and the measured cutting force F, the equivalent indentation depth $d^{\mathrm{equ}}_{\mathrm{ind}}$ was achieved with Eq. 22 for each experiment tabulated in Table 2. Hence, the theoretical predictions $\mathrm{SSD}^{\max}_{\mathrm{theo}}$ of the maximum SSD depths could be calculated with Eq. 23. Additionally, with the corresponding measurements $\mathrm{SSD}^{\max}_{\mathrm{actu}}$ of the RUM surfaces generated under various processing parameters, the relationship between $\mathrm{SSD}^{\max}_{\mathrm{theo}}$ and $\mathrm{SSD}^{\max}_{\mathrm{actu}}$ was established (Fig. 8), revealing that $\mathrm{SSD}^{\max}_{\mathrm{actu}}$ was monotone increased with $\mathrm{SSD}^{\max}_{\mathrm{theo}}$. Also, the values of K and l could be obtained through fitting the experimental data as:

$$\mathrm{SSD}^{\max}_{\mathrm{actu}} = 0.3653 \times \mathrm{SSD}^{\max}_{\mathrm{theo}} - 9.727 \tag{24}$$

Evidently, the fitting line was fairly close to the measured values of $\mathrm{SSD}^{\max}_{\mathrm{actu}}$, which validated the correctness of the proposed predictive model. Obviously, with the prediction method mentioned above, the maximum SSD depth of the RUM

surface could be indirectly evaluated by measuring the cutting force of the diamond tool, which convenience the nondestructive detection or even in situ monitoring of subsurface crack depth. Moreover, the theoretical prediction model developed in this investigation would benefit the improvement of the processing efficiency and the reduction of the processing costs.

5 Conclusions

By incorporating the probability statistics of the active machining abrasives, a theoretical predictive model for the SSD depth of the RUM surface was established with the indentation fracture mechanics of the brittle material. The prediction technique attempted to directly relate the cutting force of the diamond tool to the maximum depth of the subsurface cracks. The correctness of the proposed method was verified by the experimental measurements of Wang et al. [8]. Utilizing this prediction technique, the SSD depth of the machined surface could be precisely predicted or even online monitored through the key parameters including cutting force of the diamond tool, mechanical properties of the material, and geometrical characteristics of the abrasives. This investigation provided some potential benefits for the reduction of the processing costs and the increments of the processing efficiency.

Funding information The authors acknowledged the assistance from the programs of the Zhejiang Province Natural Science Foundation (Grant No. LY18E050028), Strategic Priority Research Program of Chinese Academy of Sciences (Grant No. XDA-Y04-02-01), Chinese Academy of Sciences and Technology Services Network program, Ningbo International Cooperation Project (Grant No. 2017D10025), Ningbo Key Industrial Project (Grant No. 2017B10007), Ningbo Natural Science Foundation (Grant No. 2018A610173 and 2019A610156), and Advanced Programs of Zhejiang Postdoctoral Science Foundation (Grant No. zj20180042).

References

1. Hed PP, Edwards DF (1987) Relationship between subsurface damage depth and surface roughness during grinding of optical glass with diamond tools. Appl Opt 26:2491
2. Wang J, Li Y (2011) Evaluating subsurface damage in optical glasses. J Eur Opt Soc Rapid 6:11001
3. Lv D, Wang H, Zhang W, Yin Z (2016) Subsurface damage depth and distribution in rotary ultrasonic machining and conventional grinding of glass BK7. Int J Adv Manuf Technol 86(9–12):2361–2371
4. Ellingson JA, Todd JA, Sun J (2001) Optical method and apparatus for detection of defects and microstructural changes in ceramics and ceramic coatings. US Patent 6285449: B1.
5. Meeder M, Mauret T, Booij S, Braat J, Fahnle O (2003) Optimization of polishing processes by using iTIRM for in situ monitoring of surface quality. Proc SPIE 5180:40–46
6. Hellier CJ (2003) Handbook of nondestructive evaluation. McGraw-Hill, New York
7. Li S, Wang Z, Wu Y (2008) Relationship between subsurface damage and surface roughness of optical materials in grinding and lapping processes. J Mater Process Technol 205(1–3):34–41
8. Wang J, Zhang C, Feng P, Zhang J (2016) A model for prediction of subsurface damage in rotary ultrasonic face milling of optical K9 glass. Int J Adv Manuf Technol 83(1–4):347–355
9. Hou ZB, Komanduri R (2003) On the mechanics of the grinding process–Part I. Stochastic nature of the grinding process. Int J Mach Tool Manu 43(15):1579–1593
10. Malkin S, Hwang TW (1996) Grinding mechanisms for ceramics. CIRP Ann Manuf Technol 45(2):569–580
11. Malkin S, Guo C (1989) Grinding technology: theory and applications of machining with abrasives. Halsted Press, New York
12. Lawn B, Wilshaw R (1975) Indentation fracture: principles and applications. J Mater Sci 10(6):1049–1081
13. Marinescu ID, Hitchiner MP, Uhlmann E, Rowe WB, Inasaki I (2016) Handbook of machining with grinding wheels. CRC Press, Wakefield
14. Cook RF, Pharr GM (1990) Direct observation and analysis of indentation cracking in glasses and ceramics. J Am Ceram Soc 73(4):787–817
15. Lambropoulos JC, Jacobs SD, Ruckman J (1999) Material removal mechanisms from grinding to polishing. Ceram Trans 102:113–128
16. Lv D, Yan C, Chen G, Liu D, Wu X, Zhu Y (2019) Mechanistic prediction for cutting force in rotary ultrasonic machining of BK7 glass based on probability statistics. Ultrasonics: doi.org/10.1016/j.ultras.2019.106006.
17. Lv D (2016) Influences of high-frequency vibration on tool wear in rotary ultrasonic machining of glass BK7. Int J Adv Manuf Technol 84(5–8):1443–1455
18. Zhang JH (2007) Study on the prediction of grind-hardened layer and its friction and wear performance. School of Shandong University, Dissertation (in Chinese)
19. Zhou X, Xi F (2002) Modeling and predicting surface roughness of the grinding process. Int J Mach Tool Manu 42(8):969–977
20. Liu DF, Cong WL, Pei ZJ (2012) A cutting force model for rotary ultrasonic machining of brittle materials. Int J Mach Tool Manu 52(1):77–84
21. Zhang C, Zhang J, Feng P (2013) Mathematical model for cutting force in rotary ultrasonic face milling of brittle materials. Int J Adv Manuf Technol 69(1–4):161–170
22. Lv D, Huang Y, Tang Y, Wang H (2013) Relationship between subsurface damage and surface roughness of glass BK7 in rotary ultrasonic machining and conventional grinding processes. Int J Adv Manuf Technol 67(1–4):613–622

Publisher's note Springer Nature remains neutral with regard to jurisdictional claims in published maps and institutional affiliations.